Journal of Applied Geophysics 103 (2014) 71–81

Contents lists available at ScienceDirect

Journal of Applied Geophysics

journal homepage: www.elsevier.com/locate/jappgeo

Simulating intense shock pulses due to asperities during fault-slip

Atsushi Sainoki *, Hani S. Mitri

Department of Mining and Materials Engineering, McGill University, 3450 University Street, Montreal, Quebec H3A 2A7, Canada

ARTICLE INFO

Article history:
Received 1 December 2013
Accepted 20 January 2014
Available online 30 January 2014

Keywords:
Fault-slip
Dynamic analysis
Fault surface asperity
Seismic wave

ABSTRACT

Seismic waves arising from fault-slip that occurs in underground mines could inflict severe damage to mine openings. Experimental results have revealed that intense shock pulses could generate due to the unloading of fault surface asperities that move apart during the fault-slip. This study focuses on examining the effect of fault surface asperities on the seismic waves arising from fault-slip. By means of a mine-wide model, dynamic analyses are carried out in order to simulate collision and unloading of fault surface asperities. Saeb and Amadei's model and Barton's shear strength model are newly implemented into constitutive models of FLAC3D code for the analyses. Parametrical study is conducted with the dynamic analyses in order to examine the most influential factor on the generation of intense seismic waves. The results reveal that stress release due to the unloading of the asperities has a significant influence on the intensity of seismic waves, while the collision of asperities, stiffness of the fault, and asperity geometry have a much lesser influence. When the stress release is large, the peak particle velocity excited by seismic waves is found to increase threefold, compared to that for fault-slip occurring along a planar surface. It indicates that significant deterioration of rockmasses could be induced due to the high particle velocities. This study has numerically confirmed the hypothesis that intense shock pulses could occur due to the unloading of fault surface asperities.

1. Introduction

In underground hard rock mines, the occurrence of rockbursts is not uncommon at great depths, and severe damage to mine openings is occasionally inflicted due to the violent failures of rockmasses (Blake and Hedley, 2003; Kaiser and Cai, 2012; White and Whyatt, 1999). Rockbursts are generally characterized into 3 types, namely strain burst, pillar burst, and fault-slip burst, according to the volume of rockmasses involved and underlying mechanism by which the rockbursts are induced (Blake and Hedley, 2003). Amongst the types of rockbursts, fault-slip bursts could cause the most significant damage to large areas that extend over several levels in underground mines given that intense seismic waves arise from the fault-slip. In such a case, seismic waves play a critical role in causing damage to mining openings, while stress changes induced by the fault-slip would be limited to areas in the vicinity of the fault.

The propagation of seismic waves excites the particle velocity of rockmass, and there is a strong correlation between the particle velocity and rockmass damage (Brinkmann, 1987; Hedley, 1992) as an increase in stresses induced by the propagation of seismic waves is proportional to the particle velocity (Brady and Brown, 1993). Thus, it is imperative to estimate peak particle velocity excited by the seismic waves in order to optimize secondary support systems for sustaining additional loads and deformations induced by the seismic waves. Although there are a number of studies that examine the influence of seismic waves on underground openings (C.M.D.M.R. Directorate, 1996), these studies are mainly based on numerical models, in which seismic waves are applied to its boundaries in the form of displacement, velocity, or acceleration. In other words, neither the mechanisms by which seismic events take place nor the locations of the seismic events are considered. Through the studies, it is certainly possible to examine the effect of seismic waves on mine openings, such as the extent of yielding zones and stress changes, whereas from a practical engineering view point, it would be difficult to propose optimized secondary support systems to accommodate the energy and deformation induced by the seismic waves since the characteristics of seismic waves expected from seismic events cannot be estimated. Hence, developing a methodology which considers source mechanisms and the locations of seismic events is of paramount importance in order to estimate the intensity of seismic waves accurately.

As described above, an appreciation of the characteristics of seismic waves arising from rockbursts is indispensable, especially when fault-slip is involved that seismically radiates a large amount of energy while inducing shear rupture and slip movements. Gay and Ortlepp (1979) conducted microscopic analysis of infilling materials on fault surfaces arising from significantly violent seismic events that took place in a deep South Africa gold mine. Ortlepp (2000) further investigated the electron micrographs of the micro-cataclastic materials showing remarkable uniformity in size and shapes of rhombic dodecahedron; and the author mentioned that the characteristics are inconceivable as

* Corresponding author. Tel.: +1 514 398 4755.
E-mail address: atsushi.sainoki@mail.mcgill.ca (A. Sainoki).

0926-9851/$ – see front matter © 2014 Elsevier B.V. All rights reserved.
http://dx.doi.org/10.1016/j.jappgeo.2014.01.009

ordinary crystallographic structures for the material. The author postulated that the particular morphology results from intense shock unloading that takes place when fault-slip takes place along a non-planar, incipient or pre-existing surface as shown in Fig. 1. In other words, violent tensile failure due to sudden reduction in normal stresses acting on the fault gives rise to the formation of the infilling materials that have the particular structure. It was further discussed that locally intense shock pulses (seismic waves) could generate as a result of the sudden release of the stresses acting on the fault where significant impact asperities occur at intervals. It is then suggested that the generation of the intense shock pulses could be one of plausible explanations for rockburst damage that is locally significant as shown in Fig. 2. It is to be noted that the term "asperity" is used to describe a saw-toothed fault surface that carries highly concentrated stress thus inducing fault-slip when the asperities are broken and sheared off in the present paper.

Although the plausible mechanism of generation of locally intense seismic waves has been proposed, a specific framework for estimating peak particle velocity expected from the intense seismic waves has not yet been established. Thus, a better understanding of the mechanism is required in order to propose practical support systems for the locally intense shock pulses. It is found from Fig. 1 that a number of factors, such as the amount of slip displacements and the size of impact asperities could have an influence on the characteristics of the generated seismic waves. A rise in normal stresses due to the impact that occurs when the asperities collide is also assumed to be an influential factor since a normal stress level prior to the unloading would more or less affect the unloading. This paper focuses on simulating the intense shock pulse, considering these factors that could affect the characteristics of the intense shock pulses, with the purpose of establishing a methodology to estimate the peak particle velocity quantitatively.

2. Methodology

In this study, examining the effect of fault surface asperities on the generation of intense shock pulse is attempted. It is admittedly ideal to develop a numerical model encompassing a fault on which asperities as shown in Fig. 1 are modelled, and to conduct numerical analysis with a numerical simulation technique that can allow for the dynamic motion of the asperities colliding and moving apart. However, shear rupture due to fault-slip in underground mines extends to large areas (Hofmann and Scheepers, 2011; Ortlepp, 2000; Swanson, 1992), and the occurrence of fault-slip is strongly dependent upon mining-induced stress state (Alber et al., 2009; Potvin et al., 2010; Sjoberg et al., 2012) as well as in-situ stress state. Thus, constructing a mine-wide scale model is essential in order to simulate fault-slip induced by mining activities. However, it is difficult to simulate fault surface asperities in the model as a significantly large number of nodal points and zones would be required for the modelling. Considering these facts, for this study, FLAC3D code (Itasca, 2009), which adopts explicit finite difference method, is utilized, and a couple of constitutive laws governing the behaviour of faults are implemented into the code with C++ programming language to simulate the intense shock pulses. Furthermore, new constants are proposed and incorporated into the constitutive models to allow for the simulation of fault-surface asperities that are difficult to actually model. The analysis procedure is first explained in detail. A detailed description of the analysis and the constitutive models is then provided.

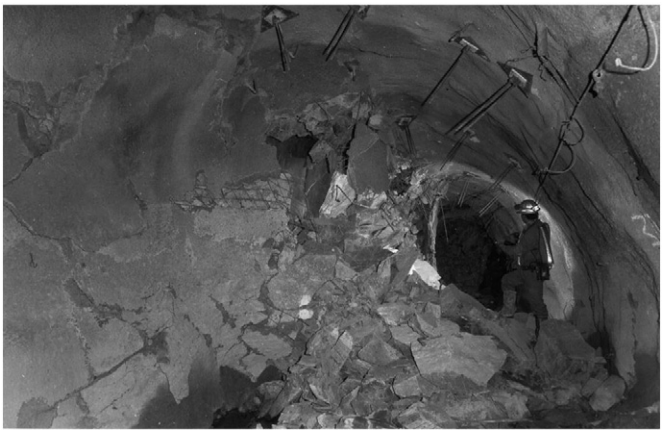

Fig. 2. Localized damage to a mine tunnel (Ortlepp, 2000).

2.1. Analysis procedure

In the present study, one static analysis and two dynamic analyses are conducted in sequence. Fig. 3 depicts the overall procedure. As shown in the figure, static analysis is first performed with a numerical model encompassing a steeply dipping, tabular orebody and fault running parallel to the orebody. During the static analysis, stopes in the orebody are extracted following mining sequences as per sublevel stoping method with delayed backfill. The reason why the extraction of stopes and backfilling are carried out prior to simulating fault-slip is to simulate mining-induced stress re-distribution on the fault. As reported in many studies (Hofmann and Scheepers, 2011; McGarr et al., 1975; Sneilling et al., 2013; White and Whyatt, 1999), the occurrence of fault-slip in underground mines is strongly associated with the stress re-arrangement, such as unclamping of fault surfaces (Castro et al., 2009), due to mining activities. Hence, the static analysis is intended to only simulate slip potential induced by the mining activities. Subsequently, dynamic analysis is carried out on the basis of the stress state obtained from the static analysis in order to simulate fault-slip. As shown in the flowchart, fault-slip resulting from asperity shear is simulated. This is due to the fact that faults in underground mines cannot be considered planar (Ortlepp, 2000; Ryder, 1988; Wallace and Morris, 1986), and as shear stress acting on the faults reaches peak shear strength, asperities on the fault are expected to be sheared off (Ryder, 1988). Excess stress determined by a difference between shear strength

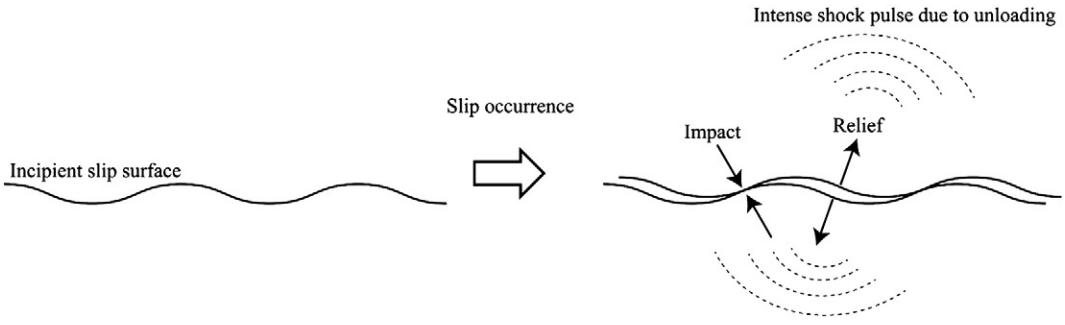

Fig. 1. Slip along a non-planar surface and generation of intense shock pulse.

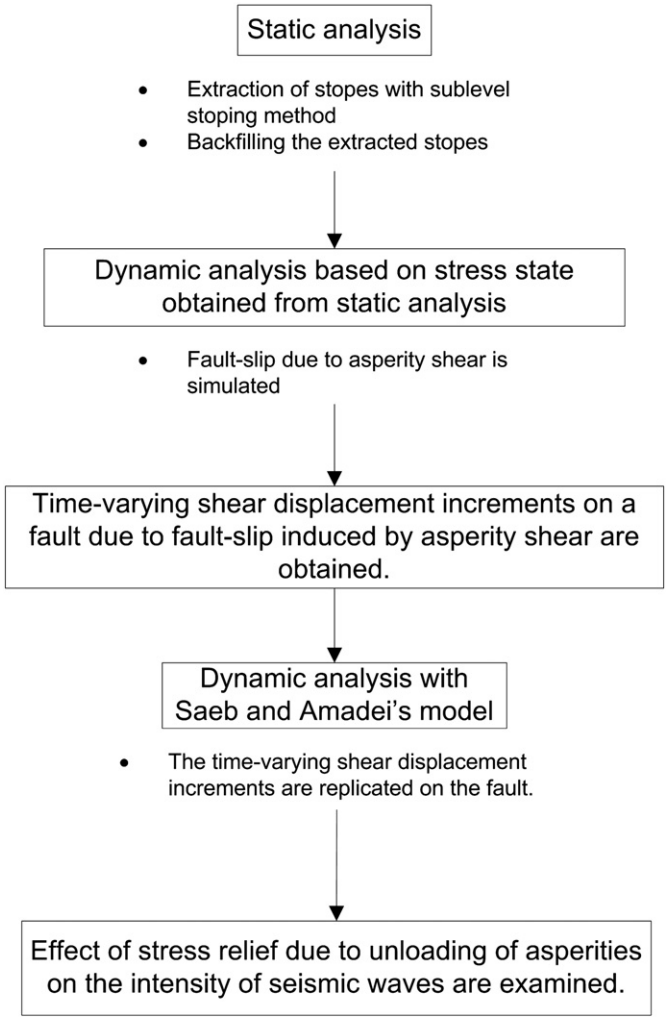

Fig. 3. Analysis procedure.

allowing for the asperities and that for planar surfaces is fault-slip driving force. Although shear rupture within intact rocks is another possible source for fault-slip (Hofmann and Scheepers, 2011), a pre-existing fault is modelled in the present study, so that asperity shear is a more plausible source for the fault-slip. Thus, a shear strength model allowing for undulation and asperities on the fault is required in order to simulate the fault-slip due to asperity shear. Regarding the shear strength model, an explanation is provided later.

After the dynamic analysis, shear displacement increments on the fault, which are caused by fault-slip due to asperity shear, are obtained with respect to dynamic time. Based on the time-varying shear displacement increments, it is attempted to examine the effect of asperities on the intensity of seismic waves. In the present study, the intensity of seismic waves is evaluated as particle velocity of rockmass obtained from the seismic waves. The reason why particle velocity is examined instead of particle acceleration is that peak particle velocity is widely used as an indication to evaluate rockmass damage induced by stress waves (Hedley, 1992; Saharan et al., 2006) due to mining-induced seismicity and rock blast vibrations. The methodology developed for this study is to apply the time-varying shear displacement increments to grip points on the fault with dynamic analysis while considering the phenomena that asperities collide with each other and move away, which are not taken into consideration during the preceding dynamic analysis. The reason why the dynamic analysis to examine the asperity effect on the intensity of seismic waves is separately performed is to conduct a parametrical study regarding fault-surface properties, such as asperity height and length, using an identical shear displacement increments. Simultaneously considering the two phenomena, namely fault-slip due to asperity shear and interactions of the asperities, makes it difficult to understand how stress release that takes place when asperities move apart is related to the generation of locally intense seismic waves. Although the two phenomena admittedly occur at the same time in real situations, the purpose of this study is to examine the effect of asperities on seismic waves. Thus, in the present study, the phenomena are simulated separately, and the asperity effect can be consequently assessed from the dynamic analysis. While a shear stress drop can be a cause for the occurrence of fault-slip, this study focuses on the generation of intense seismic waves caused by a decrease in "normal stress" due to the unloading of fault-surface asperities. Therefore, further discussion on the effect of shear stress drop is deemed unnecessary.

2.2. Shear strength model and its implementation

As mentioned above, fault-slip due to asperity shear is simulated in the present study. The only shear strength model available for FLAC3D code used to simulate fault-slip is the classical Mohr–Coulomb criterion, which is based on a friction law for planar surfaces. It is impossible to take into account asperity shear with Mohr–Coulomb criterion. Thus, a shear strength model allowing for undulation and asperities of fault surfaces needs to be employed and implemented into constitutive models of FLAC3D that can represent faults and/or fault zones. FLAC3D has two types of constitutive models that are capable of simulating slip behaviour of geological discontinuities, namely an interface model and a ubiquitous joint model. The former is widely utilized to model the geological discontinuities, which are represented as zero-thickness interfaces with the model. However, FLAC3D code does not allow users to modify the model. Thus, instead of the model, the ubiquitous joint model is employed in the present study, into which new constitutive models are incorporated with C++ programming language. It is noteworthy that the interface model and ubiquitous joint model give almost exactly the same results in terms of shear displacements, normal stress, and shear stress when compared for the same geological discontinuity (Cappa and Rutqvist, 2010). Therefore, the interface models can be replaced with the ubiquitous joint models when modelling fault-slip.

To date, a number of shear strength models for geological discontinuities with non-planar surfaces have been proposed and modified (Asadollahi and Tonon, 2010; Barton, 1973; Indraratna et al., 2005; Ladanyi and Archambault, 1970; Seidel and Haberfield, 2002). Amongst the models, Barton's shear strength model (Barton, 1973), which can allow for joint surface roughness and joint wall compressive strength, is employed and incorporated into the ubiquitous joint models of FLAC3D code. The Barton's model is given as:

$$\tau = \sigma_n \tan\left[JRC \log_{10}\left(\frac{JCS}{\sigma_n}\right) + \phi_b\right] \tag{1}$$

where σ_n and ϕ_b are effective normal stress acting on the joint and the basic friction angle of the joint, respectively; *JRC* and *JCS* are the joint roughness coefficient and joint wall compressive strength. *JRC* ranges from 0 to 20 (Barton and Choubey, 1977), where *JRC* of 20 represents the roughest, undulating tension surfaces that would normally be found in a rockmass. *JCS* can be estimated based on the uniaxial compressive strength of the rockmass, considering the degree to which the joint surfaces are weathered.

Sainoki and Mitri (2013) incorporated Barton's model into FLAC3D with the ubiquitous joint model by obtaining derivatives of the failure criterion and potential function for Barton's model. In their work, the fault-slip is driven by the excess shear stress determined by the difference between Barton's shear strength model and the classical Mohr–Coulomb criterion. The present study adopts the same methodology, whereby fault-slip is modelled by changing *JRC* from a value that represents rough fault surfaces to zero representing planar surfaces. Note that

the change in *JRC* is carried out only for areas where shear stress acting on the fault exceeds the maximum shear strength determined by Barton's model. During the dynamic analysis, shear displacement increments are recorded at each time step for all the grip points on the fault. As a result, time-varying shear displacement increments are obtained. The obtained shear displacement increments are then replicated on the fault in the form of time-varying velocity to examine the effect of asperities on the generation of intense seismic waves. Note that replicating the obtained shear displacement increments for all the grid points on the fault is significantly time-consuming; hence the replication is conducted only for grid points of which the maximum particle velocity is greater than 0.5 m/s. The criterion has been determined on the basis of a relation between the maximum particle velocity and relative shear displacements of grid points on the fault. The relative shear displacements of grid points with low particle velocities are quite small, so that such grid points do not exert a large influence on the generation of intense shock pulses. For the second dynamic analysis, a constitutive model that can simulate the shear behaviour of a dilatant rock joint is newly incorporated. Barton's shear strength model that is used to obtain time-varying shear displacement increments due to asperity shear is no longer employed during the second dynamic analysis. In the following section, the constitutive model employed for the second dynamic analysis and new constants proposed to simulate the unloading of asperities are introduced.

2.3. Method to simulate shear behaviour of a dilatant rock joint

After obtaining time-varying shear displacement increments along the entire fault, the shear displacement increments are duplicated on the fault with dynamic analysis using a different constitutive model from the preceding dynamic analysis. With the newly incorporated constitutive model, the behaviour that asperities collide and move away while releasing accumulated stresses is simulated to examine the effect of fault surface asperities on seismic waves. In order to model the behaviour, a constitutive model allowing for shear behaviour of dilatant rock joints (Saeb and Amadei, 1992) has been newly implemented into the ubiquitous joint model of FLAC3D code. It is to be noted that the ubiquitous joint model to which Saeb and Amadei's model (Saeb and Amadei, 1992) is applied does not consider slip behaviour of the fault since slip behaviour is given in the form of time-varying shear displacement increments to the grid points on the fault. The formulations proposed by the authors are given as:

$$k_{nn} = \frac{\partial \sigma_n}{\partial v} = \frac{1}{\dfrac{-uk_2}{\sigma_T}\left(1-\dfrac{\sigma_n}{\sigma_T}\right)^{k_2-1}\tan i_0 + \dfrac{V_m^2 k_{ni}}{(k_{ni}V_m-\sigma_n)^2}} \tag{2}$$

$$k_{nt} = \frac{\partial \sigma_n}{\partial u} = \frac{-\left(1-\dfrac{\sigma_n}{\sigma_T}\right)^{k_2}\tan i_0}{\dfrac{-uk_2}{\sigma_T}\left(1-\dfrac{\sigma_n}{\sigma_T}\right)^{k_2-1}\tan i_0 + \dfrac{V_m^2 k_{ni}}{(k_{ni}V_m-\sigma_n)^2}} \tag{3}$$

$$d\sigma_n = \frac{Kk_{nt}}{K-k_{nn}}du \tag{4}$$

where σ_T, V_m, i_0, and K are uniaxial compressive strength of joint wall, the maximum joint closure, the initial inclination angle of asperity, and the stiffness of host rock, respectively; k_2 is a constant and has a suggested value of 4 (Saeb and Amadei, 1992); k_{nn} and k_{nt} are two normal stiffness coefficients; u and du denote shear displacement and a shear displacement increment during a time interval, which is given from the preceding dynamic analysis. The equations above directly relate shear displacement increments to an increase in normal stress due to dilatancy resulting from the collision of asperities. Importantly, the increase in normal stress is related to the stiffness of a joint itself and surrounding rockmass. For instance, if $K = 0$, there is no increase in normal stress due to the dilatant behaviour, which corresponds with a case of shear movements occurring along a geological discontinuity in a rock slope on the ground. In that case, the slope surface is considered free boundary. On the contrary, in a case of underground mines, it is conceivable that the stiffness has more or less an influence on the rise in normal stress.

To conduct analysis considering the collision and unloading with the ubiquitous joint models, there are a couple of points to consider: (a) the ratio of area with asperities responsible for the collision to the entire fault area; (b) the behaviour of the asperities moving away. First, asperities which are responsible for the rise in normal stress would not be situated over the entire fault since a portion of the asperities is sheared off during the fault-slip; hence the ratio needs to be taken into consideration in the numerical simulation. Secondly, it is impossible to simulate the behaviour of the asperities moving away after the collision since modelling each asperity on the fault is significantly difficult on a mine-wide scale, considering the capability of personal computers available. Modelling each asperity on the fault would require a considerable number of grid points and zones in the numerical model. Thus, in the present study, stress release rate is newly proposed and incorporated in the numerical code. The amount of normal stress that decreases due to the unloading at each time step during the dynamic analysis is computed on the basis of the stress release rate. It should be noted that the stress release rate is applied only to normal stress. This is because Ortlepp (2000) indicated that tensile failure due to a sudden reduction in "normal stress" is a source for locally intense seismic waves. Furthermore, in order to conduct the parametrical study to examine the effect of fault surface asperities on seismic waves, it is indispensable to use the same shear displacement increments on the fault, which is affected by shear stress release. For these two reasons, the release in shear stress is not considered for the second dynamic analysis to simulate intense shock pulses. The aforementioned constants are implemented into codes of FLAC3D as follows:

$$d\sigma_n = r_c\frac{Kk_{nt}}{K-k_{nn}}du \because 2(n-1)L \le u \le (2n-1)L(n = 1,2,3\ldots) \tag{5}$$

$$d\sigma_n = -r_m\sigma_n \because (2n-1)L \le u \le 2nL(n = 1,2,3\ldots) \tag{6}$$

$$L = \frac{H_a}{\tan\phi_a} \tag{7}$$

where r_c represents the ratio of asperity area responsible for the increase in normal stress to the entire fault, and r_m is the release rate in normal stress while asperities move apart, respectively. L, H_a, and ϕ_a denote asperity length, asperity height, and the inclination angle of asperities as shown in Fig. 4, respectively. The rise in normal stress during the collision of asperities is computed from Eq. (5), and the reduction in normal stress during the unloading behaviour is calculated from Eq. (6). As shear displacement increments of the entire fault with respect to each time interval are obtained from preceding dynamic analysis, the increase and decrease in normal stress on the fault can be computed according to the shear displacement increments. As can be seen from Eqs. (5) and (6), it is assumed during the dynamic analysis that the collision of the asperities takes place prior to the unloading behaviour. In other words, Eq. (5) is first applied during the analysis. Eq. (6) is then applied after the total shear displacement increments reach L, which is equal to half of the asperity length as shown in Fig. 4.

3. Numerical model description

Throughout the static and dynamic analyses, the same numerical model generated with FLAC3D code is used. The model encompassing the fault and orebody on a mine-wide scale is depicted in Fig. 5. It is seen from the figure that the orebody is 22 m wide and steeply dips at 80°. The fault runs parallel to the orebody and is represented by the

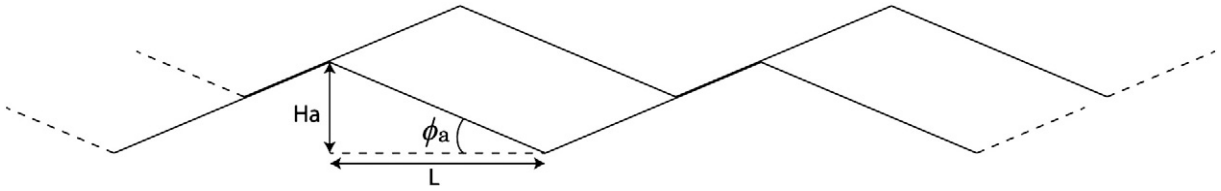

Fig. 4. Schematic illustration showing asperity geometry.

ubiquitous joint models. The distance between the fault and orebody is 30 m for this study. The length, height and width of the model have been determined after conducting preliminary analysis to examine a boundary effect on the behaviour of the fault. The intervals of each grid point are also considered, and the model has been discretized densely enough to simulate stress changes resulting from mining sequences on the fault. Although the discretization is dense enough to obtain stable results in terms of stress and displacement increments on the fault, it is too large to simulate fault surface asperities. Therefore, the method discussed in the precious section has been developed and applied to the analysis. Finally, the total numbers of grid points and zones in the model are 210798 and 195840, respectively.

The stopes extracted and backfilled during the static analysis are shown in Fig. 6. The extraction of the stopes proceeds according to the numbers illustrated in the figure, which correspond with the mining sequences of bottom-up sublevel stoping method. On each sublevel, stopes are extracted from hanging wall to footwall side. The height and strike lengths of the stopes are 30 m and 200 m, respectively. The stope strike length is admittedly longer compared to those generally planned in underground mines (Zhang and Mitri, 2008). However, modelling each stope and conducting numerical analyses to extract the stopes are significantly time-consuming. Furthermore, the purpose of the static analysis is to simulate high slip potential resulting from long-range mining sequences for the entire fault. The effect of extraction of each stope on the fault is not focused on. Therefore, the aforementioned stope geometries are modelled for the present study. As shown in the figure, the mining sequences proceed until extraction of Stope7H with the static analysis. The dynamic analysis to simulate fault-slip due to asperity shear is performed on the basis of the stress state after extracting the Stope 7H.

4. Rockmass mechanical properties and analysis conditions

The rockmass mechanical properties applied to the numerical model are based on a case study (Henning, 1998). Table 1 lists the elastic modulus, E, cohesion, C, internal friction angle, ϕ, the unit weight, γ, Poisson's ratio, ν, tensile strength, σ_T, and dilatancy angle, ψ, of the rockmasses and backfill material.

Regarding the mechanical properties of the fault, the values shown in Table 2 are applied. As explained in the previous section, fault-slip due to asperity shear is modelled during the dynamic analysis; hence joint roughness coefficient is changed from 20, which represents a joint with significantly rough surfaces, to 0 for a planar surface when the shear stress reaches the maximum shear strength. The basic friction angles of typical rock joints fall between 21° and 38° (Barton and Choubey, 1977). Considering the data, the friction angle of the fault is set at 30° for the static analysis. The dynamic coefficient of friction is generally difficult to obtain and continuously alters during the slip (Ruina, 1983). In addition, simulating the mechanism accurately is quite challenging. Hence, in the present study, the dynamic coefficient of friction is obtained by changing the friction angle to 25° for the area where a slip takes place during the dynamic analysis. As the ubiquitous joint models are used to model the fault, modulus of elasticity also needs to be considered. The modulus of elasticity is set at one-tenth of that for rockmass in hanging wall since cracks and fractures that exist in the fault zones are assumed to decrease modulus of elasticity (Brady and Brown, 1993; Budiansky and O'Connell, 1975).

A parametrical study is carried out with respect to the constants in Eqs. (2) to (7) which determine the characteristics of the collision and unloading. Table 3 shows each model for the parametric study. As shown in the table, 19 models are generated, and r_c, r_m, H_a, ϕ_a, K, and k_{ni} vary between the models. It is noteworthy that the parametrical

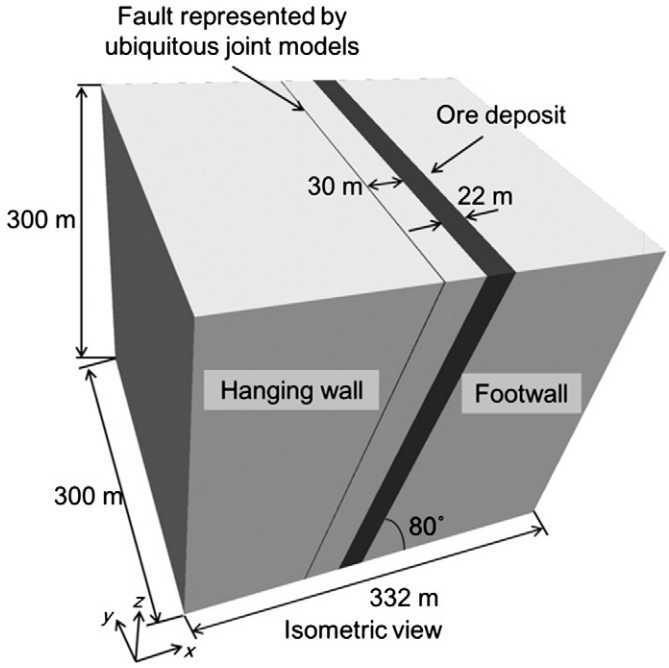

Fig. 5. Numerical model used for static and dynamic analyses.

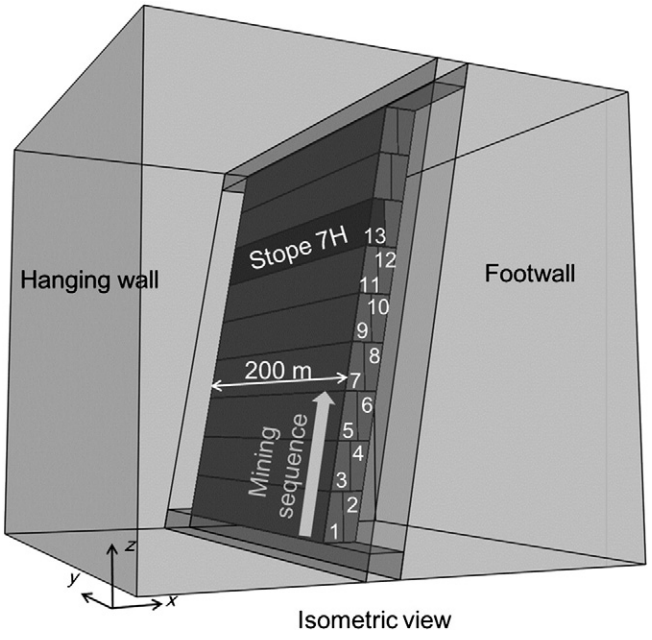

Fig. 6. Mining sequence proposed.

Table 1
Rockmass mechanical properties.

	E (GPa)	C (MPa)	ϕ (°)	ν	γ (kN/m^3)	σ_T (MPa)	ψ (°)
HW[a]	31	2.6	38	0.21	25.5	1.1	9.3
Ore	115	11.5	48	0.1	25.5	5.9	12.0
FW[b]	49	4.3	39	0.15	25.5	1.8	9.5
BW[c]	2.5	0.1	35	0.35	23.0	N/A	0.0

[a] Hanging wall.
[b] Footwall.
[c] Backfill.

study is conducted for the same time-varying shear displacement increments obtained from the preceding dynamic analysis, thus making it possible to examine the effect of the properties on the intensity of seismic waves more accurately.

The vertical in-situ stress, σ^o_v, which is in the z-direction in Fig. 5, is calculated by the overburden pressure as follows:

$$\sigma_v^o = \gamma H \tag{8}$$

where γ and H are the unit weight of the rockmass and the depth below ground surface. According to Arjang (1991), steeply dipping orebodies in the Canadian Shield have the characteristics that the maximum horizontal stress is in the direction perpendicular to orebody and the direction of minimum horizontal stress is parallel to the orebody strike. This is adopted in the present study. The magnitude of maximum and minimum horizontal stresses is determined by the following equations proposed by Diederichs (1999).

$$k_{\max} = 1 + \frac{25}{\sqrt{H}} \tag{9}$$

$$k_{\min} = 1 + \frac{8}{\sqrt{H}} \tag{10}$$

$$\sigma^o{}_{H\max} = k_{\max}\sigma_v^o \tag{11}$$

$$\sigma^o{}_{H\min} = k_{\min}\sigma_v^o \tag{12}$$

where k and σ^0_H are ratio of horizontal stress to vertical in-situ stress, and horizontal in-situ stress, respectively. In this study, the depth at the top boundary of the model is set at 3100 m below the ground surface. The value seems too large when compared to mining depths of typical Canadian mines. However, Canadian mines such as Kidd Creek in Timmins, Ontario and Laronde mine in Cadillac, Quebec have mining depths in excess of 3 km. More importantly, according to Ortlepp (2000), shear displacements during fault-slip could be up to 10 cm. The objective to carry out the first dynamic analysis is to obtain reasonable time-varying shear displacement increments during fault-slip that could be a source for the intense shock pulses. As a result of a number of preliminary analyses, it is found that the depth assumed in this study is required in order to obtain shear displacements that are comparable to those reported by Ortlepp (2000) under these conditions.

During the static analysis, model boundaries are fixed in the direction perpendicular to the boundaries. The boundary conditions are changed to viscous when dynamic analysis is carried out in order to prevent seismic waves arising from fault-slip from reflecting on the model boundaries. The timestep used for the dynamic analysis is automatically calculated based on the volume of each zone of the model, P-wave velocity obtained from rockmass mechanical properties and the face area of each zone (Itasca, 2009). Regarding the attenuation of elastic waves, local damping embodied in FLAC3D is taken. According to the manual of FLAC3D, coefficient of local damping is given as:

$$\alpha_L = \pi D \tag{13}$$

where α_L and D are the local damping coefficient and a fraction of critical damping. It operates by adding or subtracting mass from a grid point at certain times during a cycle of oscillation. Although local damping cannot capture the energy loss properly when wave forms are complicated, it enables frequency-independent damping. According to ABAQUS (2003), a fraction of critical damping for rock falls between 2 and 5%. Thus, 5% of critical damping is adopted for this study; and this damping system is deemed sufficient at this stage, considering the focus of the study.

Table 3
Models for a parametrical study.

Model	r_c	r_m	H_a (mm)	ϕ_a (°)	K (GPa/m)	k_{ni} (GPa/m)
1	0.1	0.01	10	40	2	1
2	0.01					
3	0.001					
4	0.01	0.1	10	40	2	1
5		0.001				
6	0.01	0.01	20	40	2	1
7			5			
8			1			
9	0.01	0.01	10	50	2	1
10				30		
11	0.01	0.01	10	40	20	1
12					10	
13					0.1	
14					0.05	
15	0.01	0.01	10	40	1	40
16						20
17						0.2
18						0.01
19	0	0	0	0	N/A	N/A

5. Results and discussion

As shown in Section 2.1, the first dynamic analysis is carried out to simulate fault-slip due to asperity shear while applying Barton's shear strength model. Fault-slip simulated in the first dynamic analysis has a moment magnitude of 2.28, which falls into a reasonable range as a magnitude of fault-slip or shear failure that occurs in underground mines (Alber, 2013). Relative shear displacement distribution on the fault is similar to that simulated with the same methodology (Sainoki and Mitri, 2013), albeit its magnitude differs. The obtained time-varying shear displacement increments are used as an input parameter for the second dynamic analysis. The results obtained from the second dynamic analysis, in which the collision and unloading of fault surface asperities are simulated with Eqs. (2) to (7), are discussed in this section. First, the propagation of seismic waves obtained from Model 19 assuming a completely planar surface is depicted in Fig. 7 in order to give a general idea of how seismic waves propagate from the hypocenter. Particle velocities excited by the seismic waves arising from the fault-slip are shown on sectional views of the model along y = 150 m. As shown in the figure, fault-slip takes place in the vicinity of the stope

Table 2
Mechanical properties of fault.

	E (GPa)	JRC	JCS (MPa)	ϕ (°)	C (MPa)	ν	γ (kN/m^3)	σ_T (MPa)	ψ (°)
Static analysis	3.1	20	120	30	0	0.21	25.5	0	0
After slip occurs during dynamic analysis	3.1	0	120	25	0	0.21	25.5	0	0

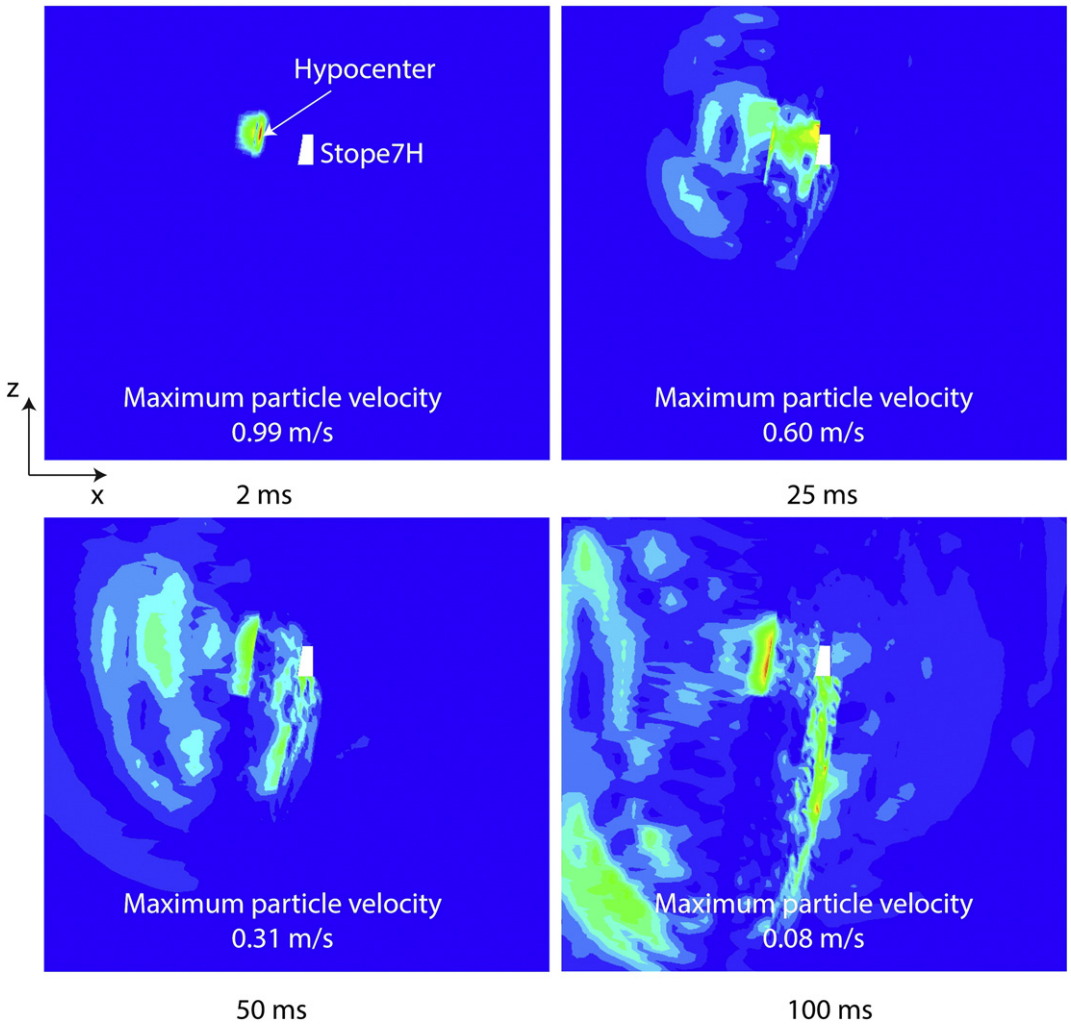

Fig. 7. Particle velocities excited by propagation of seismic waves arising from fault-slip on sectional views along y = 130 m for Model 19.

extracted immediately before the dynamic analysis. The maximum particle velocity is 0.99 m/s 2 ms after the onset of the analysis. After 25 ms, the seismic waves propagate around the hypocenter extensively, and the maximum particle velocity decreases to 0.60 m/s. Finally, the propagation of seismic waves increases particle velocity across the whole model, and the maximum velocity drops to 0.08 m/s. The particle velocity of 0.99 m/s could cause damage to intact hard rock (Saharan et al., 2006), while severe damage is not expected from the particle velocity of 0.60 m/s. This figure indicates that the particle velocity of the rockmass takes the maximum value immediately after the onset of fault-slip; and it follows that the particle velocity rapidly decreases as seismic waves propagate through the rockmass.

Fig. 8 depicts the propagation of seismic waves for Model 2, which considers the collision and unloading of fault surface asperities. As shown in the figure, the maximum particle velocity for Model 2 is the same as that for Model 1 at the beginning of the dynamic analysis. However, it is seen from the figure that a difference in the maximum particle velocity between the models becomes evident as time goes by. 25 ms after the onset of the analysis, the maximum particle velocity increases rapidly to 2.90 m/s, and comparable high particle velocity continues at least until 50 ms. These particle velocities are significantly greater than those for Model 19, in which a planar surface is assumed. More importantly, the particle velocity is high enough to cause severe damage to rockmass (Hedley, 1992; Saharan et al., 2006). It is considered that the results reflect sudden stress relief due to the unloading of fault surface asperities. In other words, for Model 2, shear displacement increments around areas where the intense shock pulses generate become large enough that Eq. (6) is applied instead of Eq. (5). Although the maximum particle velocity eventually decreases to 0.47 m/s after 100 ms, the value is still greater than that for Model 19. These long-lasting high particle velocities could cause more deterioration of rockmass in the environs of the fault. Peak particle velocities found from figures are 2.90 m/s and 0.99 m/s for Model 2 and 19 during the seismic events, respectively. Hence, the results suggest that a sudden stress drop due to the unloading of fault surface asperities could cause extremely high particle velocities that induce severe damage to the rockmass. The simulated extremely high particle velocity coincides with that observed in deep gold mines (e.g. peak particle velocity of 3 m/s at Tau Tona gold mine and PPV of 2.3 m/s at Mponeng gold mine reported by Milev et al. (2002)).

Results of the parametrical study conducted for the parameters in Table 3 are shown in Fig. 9. In the figure, the maximum particle velocities at certain times for each model are compared with those for Model 2. Hence, the result obtained from Model 2 is repeatedly shown in Fig. 9a to f for the comparison. Fig. 9a shows the results obtained from models with different r_c in Eq. (5), which denotes a ratio of asperity area responsible for the collision to the entire fault area. As can be seen from the figure, the maximum particle velocities for each model almost coincide. Although a slight difference in the maximum particle velocity amongst the models is observed, it can be negligible, considering absolute values of the particle velocities. Thus, these results indicate that the collisions of fault surface asperities during the fault-slip do not significantly affect the intensity of seismic waves in terms of particle

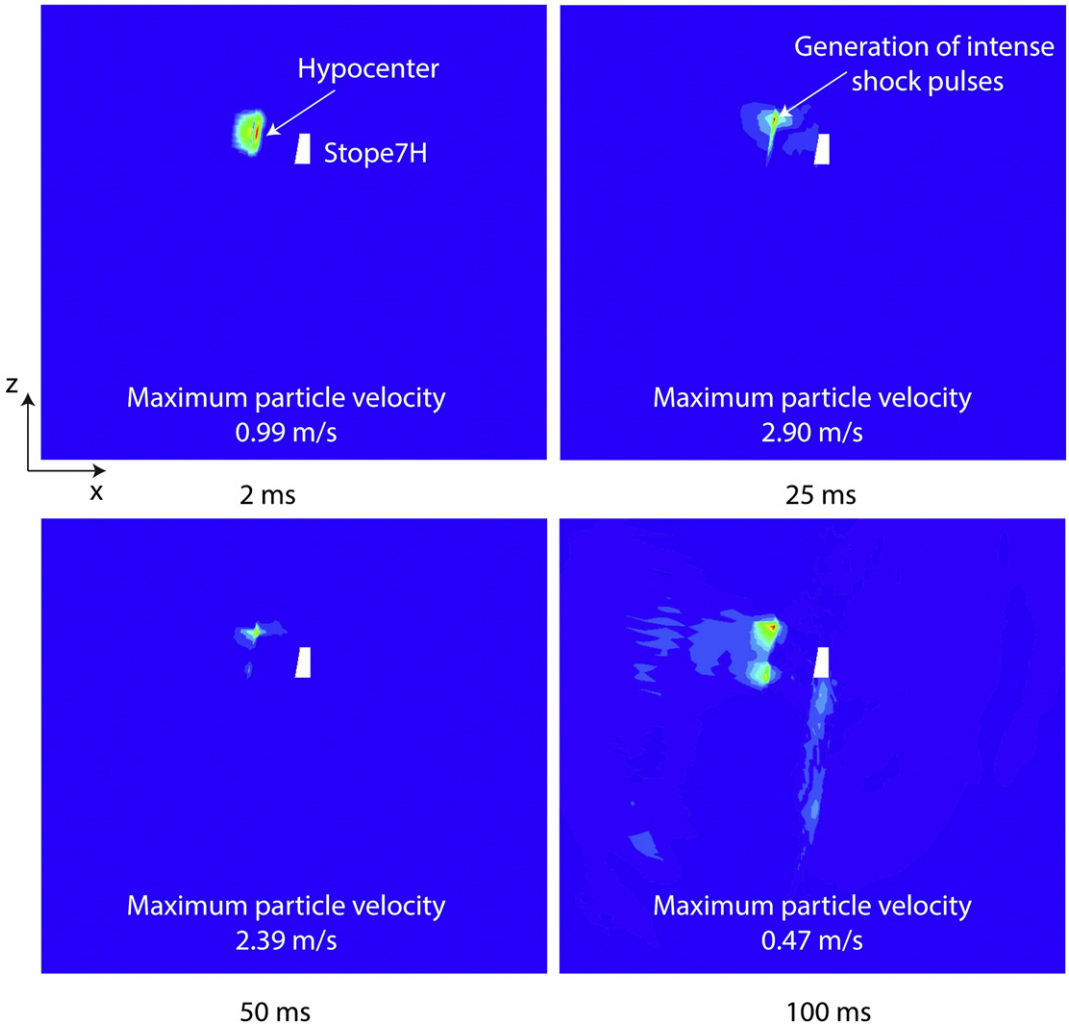

Fig. 8. Particle velocities excited by propagation of seismic waves arising from fault-slip on sectional views along y = 130 m for Model 2.

velocity, at least under the conditions shown in Table 3. The increase in normal stress due to the collision is also a function of the stiffness of surrounding rockmasses, K, and the stiffness of the fault, k_{ni}, as can be seen from Eqs. (2) to (4). For the parametrical study, K ranges from 0.05 GPa/m to 20 GPa/m, and k_{ni} varies between 0.1 GPa/m and 40 GPa/m. It is found from Fig. 9e and f that the parameters also do not exert a large influence on the intensity of seismic waves.

In contrast to these results, there are evident differences in the maximum particle velocities between models shown in Fig. 9b, c, and d. Fig. 9b shows results obtained from models with different r_m in Eq. (6), which denotes a stress release rate during the unloading of fault surface asperities. For the parametrical study, r_m ranges from 0.001 to 0.1. As shown in Fig. 9b, the maximum particle velocity is 3.9 m/s 50 ms after the onset of dynamic analysis when $r_m = 0.1$ (Model 4). The particle velocity is almost 13 times higher than that of Model 19 at that time. Even in the case that $r_m = 0.01$, the particle velocity is still significantly higher than that obtained from Model 19. On the other hand, when r_m decreases to 0.001, the maximum particle velocities are approximately same as those for Model 19 shown in Fig. 7. These results imply that the stress release rate, r_m, has a significant influence on the intensity of seismic waves, especially when the rate is large. These results further indicate the importance of carrying out numerical simulation that relates the stress release rate, r_m, to actual stress release that would take place along fault surface asperities, using a numerical model in which asperities are modelled on an actual size. When the relation is established, it is possible to estimate the high particle velocity excited by intense shock pulses accurately. Fig. 9c shows the effect of asperity height, which varies between 1 mm and 20 mm for the parametrical study, on the intensity of seismic waves. It is found from the figure that the maximum particle velocities do not differ between the models until 2 ms. This is because the influence of collisions on the seismic waves is negligible as indicated in Fig. 9a, e, and f. After 5 ms, the difference in the maximum particle velocity between the models becomes clear. It is found from Fig. 9c that particle velocity takes the peak value 10 ms after the onset of the analysis when $H_a = 1$ mm and 5 mm. On the other hand, when $H_a = 10$ mm, particle velocity reaches the peak value 25 ms after the onset of the analysis. In addition, when $H_a = 20$ mm, a significant increase in particle velocity is not observed during the dynamic analysis. It is considered that these characteristics reflect asperity length, L, since the unloading of fault surface asperities is simulated after shear displacement increments reach the asperity length (see Eq. (6)), which is dependent upon asperity height and asperity inclination angle. Therefore, a similar tendency can be found in Fig. 9d, in which models with different asperity inclination angles are compared. As can be seen in the figure, in the case that asperity inclination angles are large, particle velocity takes the maximum value earlier, compared with the model with a low asperity inclination angle. More importantly, although the height and inclination angle of asperity contribute to the characteristics of seismic waves, peak particle velocity observed during the seismic events is not significantly affected by the parameters. For example, for Model 2, peak particle velocity is 2.90 m/s as shown in Fig. 8; and for Model 8, peak particle velocity is

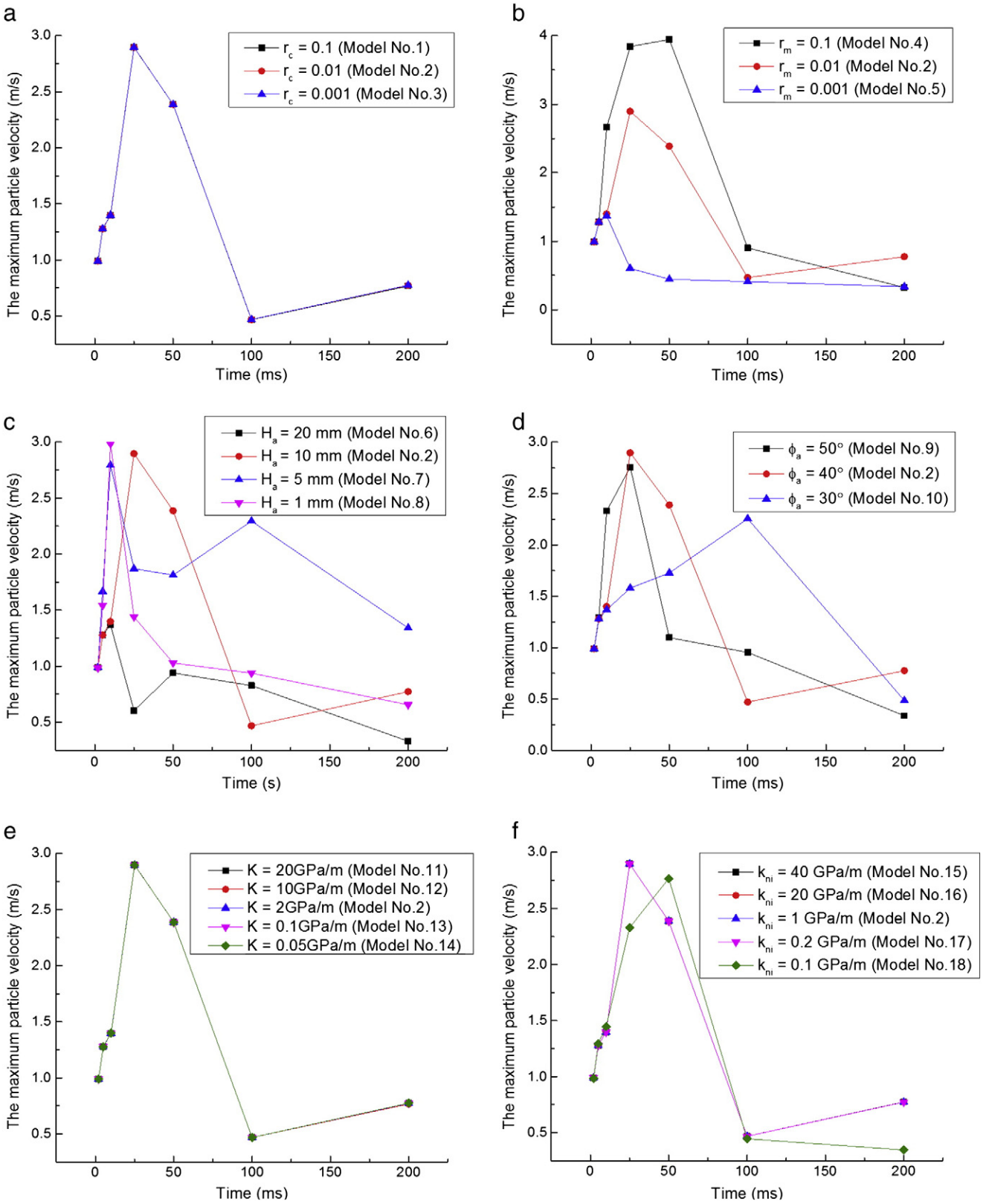

Fig. 9. Effect of fault-surface properties and boundary conditions on the intensity of seismic waves: a) effect of asperity area ratio, b) effect of stress release rate, c) effect of asperity height, d) effect of asperity inclination angle, e) effect of the stiffness of rockmass, and f) effect of the initial shear stiffness of asperities.

2.98 m/s. The difference in the particle velocity is 0.08 m/s, which is quite small when compared with the influence exerted by stress release rates as shown in Fig. 9b.

Finally, peak particle velocity normalized on the basis of that for Model 19 is shown in Fig. 10. The peak particle velocity represents the maximum particle velocity at the observation time shown in Fig. 9

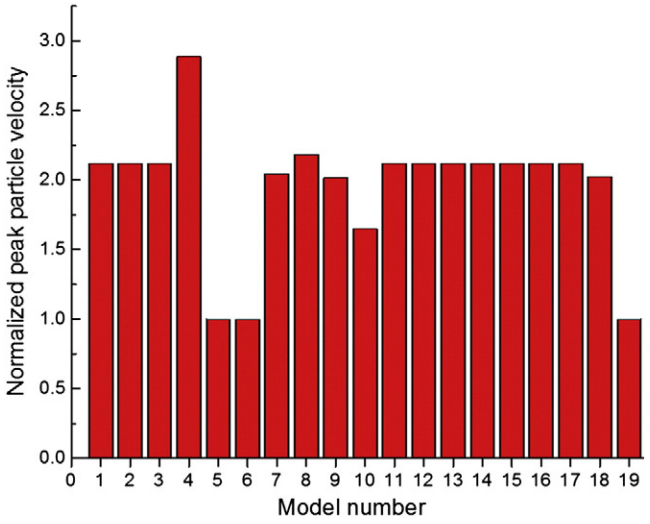

Fig. 10. Peak particle velocity normalized on the basis of Model 19.

during seismic events. As discussed above, it can be seen from the figure that the influence of fault geometry, such as the height and inclination angle of asperity, on the intensity of seismic waves is not significant. For instance, although peak particle velocity for Model 8 is almost twice as large as that for Model 19, the difference is mainly due to stress release rates because there is not a large difference in peak particle velocity between Models 7 and 8 as shown in Fig. 9c. Likewise, r_c and the stiffness of surrounding rockmass and the fault do not have a large influence on peak particle velocity (see Models 1 to 3 and 11 to 18). Evidently, the most influential factor to peak particle velocity excited by seismic waves is a stress release rate, r_m. According to the figure, peak particle velocity for Model 4, in which r_m is set at 0.1, is approximately 3 times larger than that for a planar surface. The high peak particle velocity is considerable and large enough to cause significant damage to rockmasses (Saharan, 2004), thereby suggesting that conducting further analysis to relate a stress release rate with an actual stress release rate is of paramount importance. Although the results obtained from this study show that asperity surface geometry does not significantly affect the characteristics of seismic waves in terms of peak particle velocity, the stress release rate, r_m, is presumed to be inherently related to fault surface geometry. Due to the limitations of numerical simulation approach attempted for this study, the relation cannot be obtained from the conducted analyses. Hence, further analysis is required for a better understanding of the relation. When the relation is developed, the simulation technique proposed in the present paper can be an efficient method to estimate extremely high peak particle velocity that could be induced by seismic waves arising from fault-slip that occurs along a fault with significant asperities. In addition, developing the relationship between the stress release rate and asperity surface geometry will make it possible to calibrate a model by carrying out back analysis, using field measurements and seismic source parameters.

6. Conclusions

The effect of fault surface asperities on the intensity of seismic waves arising from fault-slip is examined with a mine-wide model encompassing a fault in the vicinity of a multi-level mining zone of a steeply dipping tabular orebody. In order to simulate fault-slip, Barton's model is newly incorporated into FLAC3D with C++ programming language. In addition, Saeb and Amadei's model is implemented to simulate the collision of fault surface asperities during the fault-slip. A sudden stress drop due to unloading of the asperities during fault-slip is simulated by implementing a stress release rate into the constitutive model. After initiating stress re-distribution due to a sequence of stope extractions with static analysis, dynamic analysis takes over out with the newly developed constitutive models.

The results obtained from the analysis show that the effect of collision of fault surface asperities on the intensity of seismic waves is negligible. On the other hand, the unloading of fault surface asperities has a significant influence on the characteristics of seismic waves when the stress release rate is large. The results also show that high particle velocity could continue for a long period of time due to the unloading, which could cause the deterioration of the rockmass. More importantly, when the stress release rate is high, the peak particle velocity could be three times higher than that obtained from a model with planar surface. In addition, the velocity is found to be high enough to cause severe damage to rockmasses. It can be concluded that the stress release rate is the most influential factor that affects the intensity of seismic waves. However, due to the limitation of numerical simulation approach employed in the present study, the relation between the stress release rate and the geometry of the asperities of the undulating fault surfaces is still unclear. Hence, conducting further study is recommended in order to establish that relation. When such relation is derived, the simulation technique proposed in the present study can be quite an efficient method to estimate peak particle velocity excited by intense shock pulses arising from the unloading of fault surface asperities.

Acknowledgement

This work is financially supported by a grant from the Natural Science and Engineering Research Council of Canada (NSERC) — Discovery Grant Program, and McGill University (MEDA Fellowship Program); the authors are grateful for their support.

References

ABAQUS, 2003. ABAQUS online documentation: Ver 6.4–1. Dassault Systemes, France.
Alber, M., 2013. Strength of faults—a concern for mining engineers? In: Kwasniewski, Lydzba (Ed.), Eurock. Taylor & Francis Group, London, Poland, pp. 545–550.
Alber, M., Fritschen, R., Bischoff, M., Meier, T., 2009. Rock mechanical investigations of seismic events in a deep longwall coal mine. Int. J. Rock Mech. Min. Sci. 46, 408–420.
Arjang, B., 1991. Pre-mining stresses at some hard rock mines in the Canadian Shield. CIM Bull. 84, 80–86.
Asadollahi, P., Tonon, F., 2010. Constitutive model for rock fractures: revisiting Barton's empirical model. Eng. Geol. 113, 11–32.
Barton, N., 1973. Review of a new shear-strength criterion for rock joints. Eng. Geol. 7, 287–332.
Barton, N., Choubey, V., 1977. The shear strength of rock joints in theory and practice. Rock Mech. 10, 1–54.
Blake, W., Hedley, D.G.F., 2003. Rockbursts case studies from North America Hard-Rock Mines. Society for Mining, Metallurgy, and Exploration, Littleton, Colorado, USA.
Brady, B.H.G., Brown, E.T., 1993. Rock mechanics: for underground mining. Chapman & Hall, London.
Brinkmann, J.R., 1987. Separating shock wave and gas expansion breakage mechanism. 2nd International Symposium rock fragmentation by blasting.
Budiansky, B., O'Connell, R.J., 1975. Elastic moduli of a cracked solid. Int. J. Solids Struct. 12, 81–97.
C.M.D.M.R. Directorate, 1996. Canadian rockburst research program, 1990–1995: a comprehensive summary of five years of collaborative research on rockbursting in hardrock mines. CAMIRO Mining Division, Sudbury, Ontario.
Cappa, F., Rutqvist, J., 2010. Modeling of coupled deformation and permeability evolution during fault reactivation induced by deep underground injection of CO2. Int. J. Greenhouse Gas Control 5, 336–346.
Castro, L.A.M., Carter, T.G., Lightfoot, N., 2009. Investigating factors influencing fault-slip in seismically active structures. 3rd CANUS Rock Mechanics Symposium, Toronto.
Diederichs, M.S., 1999. Instability of hard rockmass: the role of tensile damage and relaxation in. University of Waterloo, Waterloo, Canada.
Gay, N.C., Ortlepp, W.D., 1979. Anatomy of a mining-induced fault zone. Geol. Soc. Am. Bull. 90, 47–58.
Hedley, D.G.F., 1992. Rockburst handbook for Ontario hard rock mines Minister of supply and services Canada.
Henning, J., 1998. Ground control strategies at the Bousquet 2 mine. Mining & Materials Engineering. McGill University, Montreal, QC, Canada.
Hofmann, G.F., Scheepers, L.J., 2011. Simulating fault slip areas of mining induced seismic tremors using static boundary element numerical modelling. Min. Technol. 120, 53–64.
Indraratna, B., Welideniya, S., Brown, T., 2005. New shear strength criterion for infilled rock joints. Geotechnique, 55. Institution of Civil Engineerings, pp. 215–226.
Itasca, 2009. FLAC3D—fast Lagrangian analysis of continua. Itasca Consulting Group Inc., U.S.A.

Kaiser, P.K., Cai, M., 2012. Design of rock support system under rockburst conditions. J. Rock. Geotech. Eng. 4, 215–227.
Ladanyi, B., Archambault, G., 1970. Simulation of shear behaviour of a jointed rock mass. In: Somerton, W.H. (Ed.), Eleventh Symposium on Rock Mechanics NY, society of Mining Engineers, 1970. The University of California, Berkeley, California, pp. 105–125.
McGarr, A., Spottiswoode, S.M., Gay, N.C., 1975. Relationship of mine tremors to induced stresses and to rock properties in the focal region. Bull. Seismol. Soc. Am. 65, 981–993.
Milev, A.M., Spottiswoode, S.M., Noble, B.R., Linzer, L.M., Zyl, M.V., Daehnke, A., Acheampong, E., 2002. The meaningful use of peak particle velocities at excavation surfaces for the opetimisation of the rockburst criteria for tunnels and stopes. Safety in Mines Research Advisory Committee.
Ortlepp, W.D., 2000. Observation of mining-induced faults in an intact rock mass at depth. Int. J. Rock Mech. Min. Sci. 37, 423–426.
Potvin, Y., Jarufe, J., Wesseloo, J., 2010. Interpretation of seismic data and numerical modelling of fault reactivation at El Teniente. Reservas Norte sector, 119, pp. 175–181.
Ruina, A., 1983. Slip instability and state variable friction laws. J. Geophys. Res. 88, 10359–10370.
Ryder, J.A., 1988. Excess shear stress in the assessment of geologically hazardous situations. J. South Afr. Inst. Min. Metall. 88, 27–39.
Saharan, M.R., 2004. Dynamic modelling of rock fracturing by destress blasting. Mining & Materials Engineering. McGill University, Montreal, QC, Canada.
Saeb, S., Amadei, B., 1992. Modelling rock joints under shear and normal loading. Int. J. Rock Mech. Min. Sci. 29, 267–278.
Saharan, M.R., Mitri, H.S., Jethwa, J.L., 2006. Rock fracturing by explosive energy: review of state-of-the-art. Fragblast 10, 61–81.
Sainoki, A., Mitri, H.S., 2013. Comparative study of shear strength models for fault-slip analysis. In: Feng, X.-T., Hudson, J.A., Tan, F. (Eds.), Sinorock Taylor & Francis Group, London, Shanghai, pp. 551–556.
Seidel, J.P., Haberfield, C.M., 2002. A theoretical model for rock joints subjected to constant normal stiffness direct shear. Int. J. Rock Mech. Min. Sci. 39, 539–553.
Sjoberg, J., Perman, F., Quinteiro, C., Malmgren, L., Dahner-Lindkvist, C., Boskovic, M., 2012. Numerical analysis of alternative mining sequences to minimize potential for fault slip rockbursting. Min. Technol. 121, 226–235.
Sneilling, P.E., Godin, L., McKinnon, S.D., 2013. The role of geologic structure and stress in triggering remote seismicity in Creighton Mine, Sudbury, Canada. Int. J. Rock Mech. Min. Sci. 58, 166–179.
Swanson, P.L., 1992. Mining-induced seismicity in faulted geologic structures: an analysis of seismicity-induced slip potential. Pure Appl. Geophys. 139, 657–676.
Wallace, R.E., Morris, T., 1986. Characteristics of faults and shear zones in deep mines. Pure Appl. Geophys. 124, 107–125.
White, B.G., Whyatt, J.K., 1999. Role of fault slip on mechanisms of rock burst damage, Lucky Friday Mine, Idaho, USA. 2nd Southern African Rock Engineering Symposium. Implementing Rock Engineering Knowledge, Johannesburg, S. Africa.
Zhang, Y., Mitri, H., 2008. Elastoplastic stability analysis of mine haulage drift in the vicinity of mined stopes. Int. J. Rock Mech. Min. Sci. 45, 574–593.